

Radiation Heating of a Nb₃Sn Cos-Theta Separation Dipole

S. Yadav, V.V. Kashikhin and A.V. Zlobin
*Fermi National Accelerator Laboratory
MS 316, PO Box 500, Batavia, IL, USA*

Abstract — Inner triplets in the LHC interaction regions are among the systems which will limit the LHC luminosity. One of the possible options for a new higher luminosity IR design is a double-bore inner triplet with beam separation dipoles placed in front of the focusing quadrupoles. The high radiation load on such a dipole from the interaction point will determine the workability of the magnet. This note presents the results of preliminary thermal analysis for the Fermilab's Nb₃Sn single-bore cos-theta design of the separation dipole based on the energy deposition calculations performed with the MARS code.

1. Introduction

The future LHC upgrades assume an increase of the luminosity by an order of magnitude with respect to the nominal luminosity of $10^{34} \text{ cm}^{-2} \text{ s}^{-1}$ using an optimized interaction region (IR) design. One of the possible approaches to the new IR design is a double-bore inner triplet with high-field large-aperture separation dipoles placed in front of the quadrupoles [1]. The luminosity increase will lead to the higher heat depositions in the IR magnets. For the IR layout with the separation dipole placed in front of the inner triplet the problem of radiation heating and radiation dose become critical and require special attention.

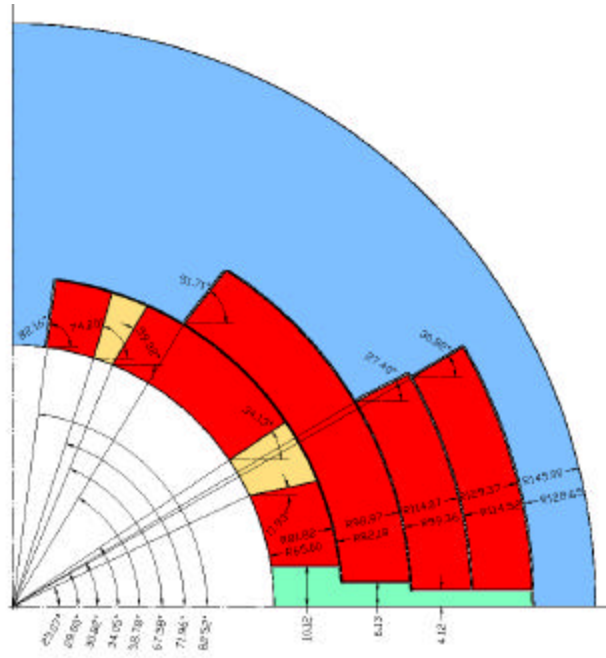
Detailed energy deposition calculations in high-field large-aperture separation dipoles of two designs have been recently performed using MARS14 code in order to determine the workability of the magnets in the dipole-first IR design for two types of separation dipole [2]. These calculations have shown that for the block type dipole design with the midplane gaps developed by BNL heat depositions in the coil are on the same level as in present NbTi IR quadrupoles whereas in traditional cos-theta dipole design developed at Fermilab even with large mid-plane spacers the heat depositions in the coil are more than 20 times higher than the peak power in the present quadrupoles at a luminosity of $10^{34} \text{ cm}^{-2} \text{ s}^{-1}$ [3]. Although the results of heat deposition analysis look more favorable for the first design approach, the second approach looks more practical and robust at present time. Therefore solution of the heat deposition and coil cooling problems for the cos-theta dipole design is an important task. This note presents the results of preliminary thermal analysis for a Nb₃Sn single-bore cos-theta design of the separation dipole for the 2nd generation LHC IRs.

2. Magnet cross-section.

The cross-section of large-aperture high-field separation dipole developed at Fermilab is shown in Figure 1. Magnet parameters at temperature of 4.5 K for Nb₃Sn strands with $J_c(12\text{ T}, 4.2\text{ K}) = 3000\text{ A/mm}^2$ are summarized in Table 1.

Table 1: Magnet parameters

Parameter	Units	Value
Coil aperture	mm	130
Number of layers	-	4
Nominal bore field	T	13.6
Quench bore field	T	15.7
Quench peak field	T	16.3
Conductor cross-section area	cm ²	119.1
Yoke outer diameter	mm	~1000



3. Heat Depositions

The MARS calculations of radiation-induced heat depositions in the magnet were performed for the luminosity of $10^{35} \text{ cm}^{-2} \text{ s}^{-1}$ [2]. The calculated distribution of heat depositions in the D1 coil is shown in Figure 2. The data are reported in mW/mm^3 for the quadrant of the coil cross-section with the largest heat deposition.

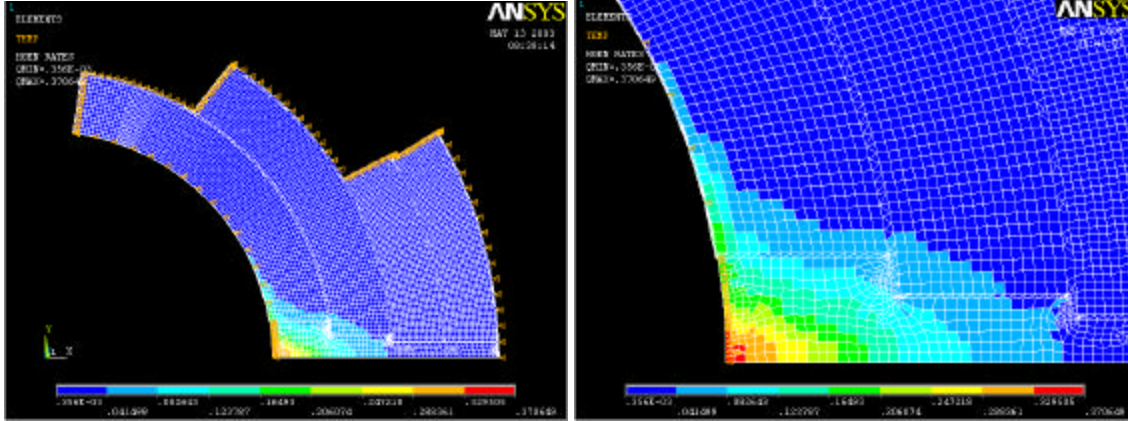


Figure 2: Distribution of the radiation heat load in the coil elements in mW/mm^3 .

According to the calculations the peak power density on the mid-plane of the cos-theta dipole magnet reaches 49 mW/g . This peak occurs in the copper spacers at the mid-plane. The maximum power density in the coils is 13 mW/g , which is more than 20 times larger than the peak power in the quadrupoles in the baseline LHC IR at a luminosity of $10^{34} \text{ cm}^{-2} \text{ s}^{-1}$ [3]. This high level of heat load presents a significant challenge for coil cooling.

4. 2D ANSYS thermal model and material properties

Two-dimensional finite element thermal model of the coil cross-section was developed using ANSYS code. The materials used in the modeled geometry are shown with different colors and different numbers in Figure 3. The cable insulation thickness is 0.2 mm , while the interlayer insulation thickness is 0.5 mm . The insulation thickness above the midplane block is 0.5 mm .

Thermal conductivity in W/m/K at 1.9 K for materials used in the dipole design is reported in Table 2. It is assumed that the perimeter of the coil is in contact with superfluid HeII with the nominal temperature of 1.9 K .

Table 2: Thermal conductivity at 1.9 K for different materials.

Material	K_r , W/m/K	K_z , W/m/K
Inner cable blocks	5	0.018
Outer cable blocks	5	0.018
Wedge	140	140
Mid-plane spacer	140	140
Insulation	0.02	0.02

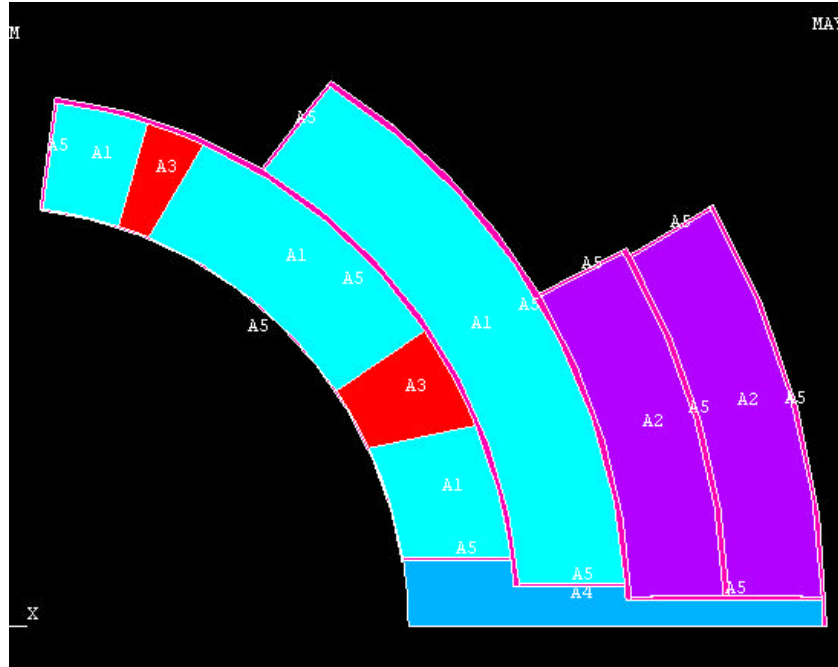


Figure 3: 2D ANSYS thermal model of the dipole coil.

5. Results and discussion

The results of calculation of temperature profile in the coil for two cases without (left) and with (right) HeII penetration inside the midplane spacer are presented in Figure 4. A constant temperature of 1.9 K is applied all along the boundary shown by yellow arrows in the above plot. The hottest point in the coil in both cases is located in the 2nd coil layer near the midplane. The maximum temperature in the hottest point reaches the level of 27.7 K and 24.8 K respectively, which is much higher than the Nb₃Sn critical temperature. As it can be seen, the 1.9 K boundary on the coil midplane surface does not lead to a significant decrease of the maximum coil temperature due to relatively low thermal conductivity of the coil in the azimuthal direction.

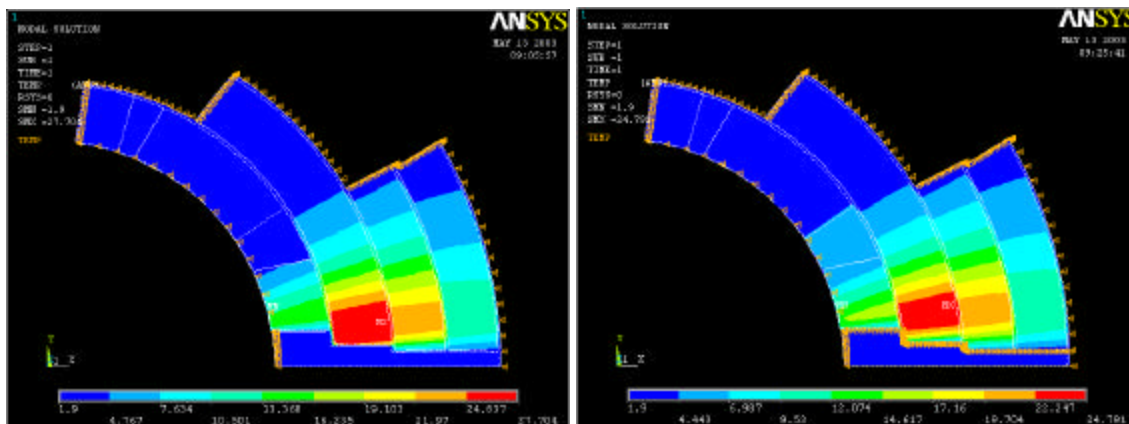


Figure 4: Temperature profile without and with HeII penetration inside the midplane spacer.

To study the effect of thermal conductivity of coil insulation system on the coil maximum temperature the thermal conductivity of the insulation (both cable and interlayer) was decreased from 0.02 W/m/K to 0.01 W/m/K. The results of calculation of temperature profile in the coil without and with HeII penetration inside the midplane spacer are presented in Figure 5. As in the previous case the hottest point in the coil for both boundary conditions is located in the 2nd coil layer near the mid-plane. The maximum temperature in the hottest points increased to 48.3 K and 40.7 K respectively. These results indicate that the maximum temperature in the coil is very sensitive to the thermal properties of insulation. All further calculations use thermal conductivity of 0.02 W/m/K for the cable and interlayer insulation.

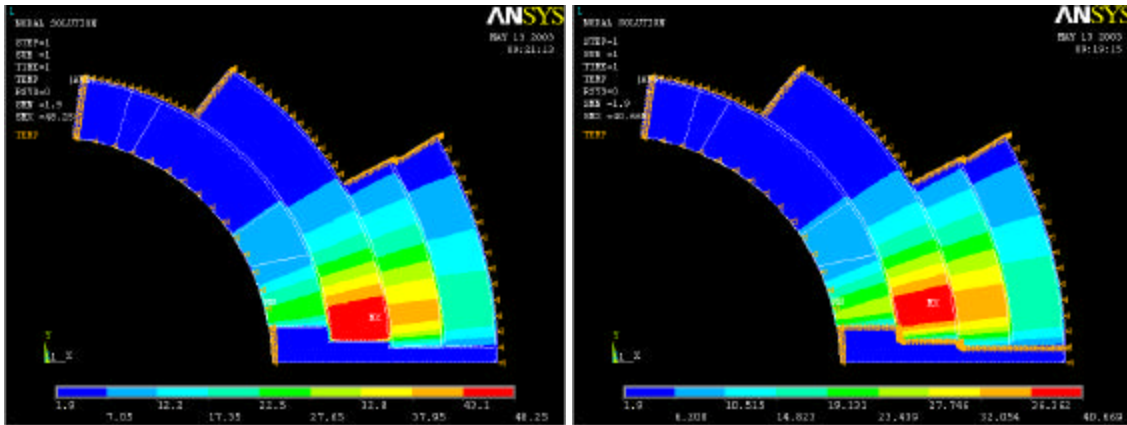


Figure 5: Temperature profile for the case where thermal conductivity of cable and interlayer insulation is 0.01 mW/mm/K and two different sets of boundary conditions.

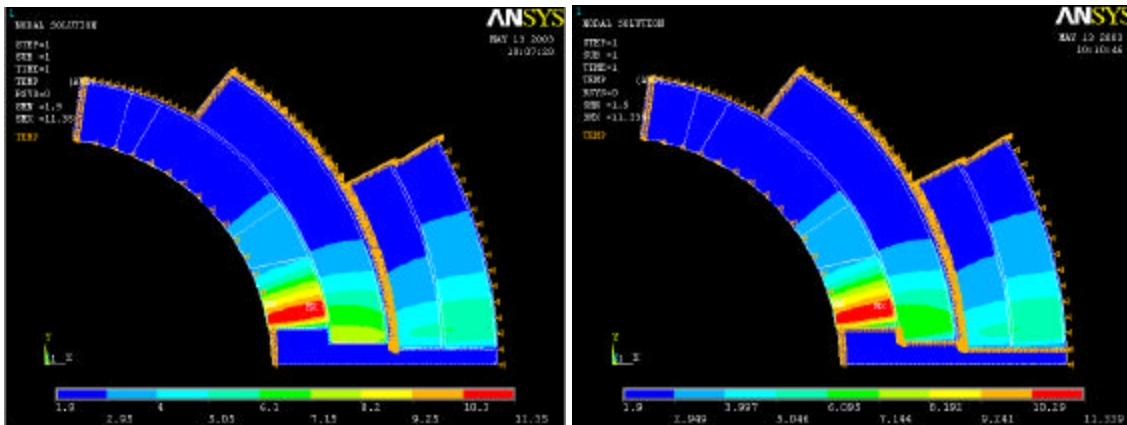


Figure 6: Temperature profile for the case with interlayer cooling and a different set of applied temperature boundary conditions in the coil midplane.

Four-layer coil design allows introducing interlayer cooling channels between the two impregnated double-layer Nb₃Sn coils in order to reduce the coil maximum temperature. To study the effect of the interlayer channels the thermal conductivity of the insulation (both cable and interlayer) was decreased from 0.02 W/m/K to 0.01 W/m/K in order to take into account the 50% contact surface with He in the channel due to “fishbone” spacer. The results of calculation of temperature profile in the coil with the interlayer

cooling channels without and with HeII penetration inside the mid-plane spacer are presented in Figure 6. The hottest point in the coil in both cases moved in the innermost layer. The maximum temperature in the hottest points decreased to 11.35 K and 11.34 K respectively which is still above the conductor critical temperature in these points at the nominal operation current.

An additional reduction of the coil maximum temperature in the innermost layer could be achieved by removing (perforating) the cable insulation on the inner surface of the mid-plane block. The temperature profile for this case is shown in Figure 7 (left). As it can be seen the hottest point has moved to the 2nd coil layer and the maximum coil temperature reduced to 7 K while the cable critical temperature at the nominal operation current in the hottest point is 9.2 K. The same level of coil maximum temperature (6.6 K) but in the innermost layer could be achieved by reducing the heat load by a factor of two (right plot in Figure 7) which is also below the coil critical temperature of 7.1 K in the hottest point at the magnet nominal current.

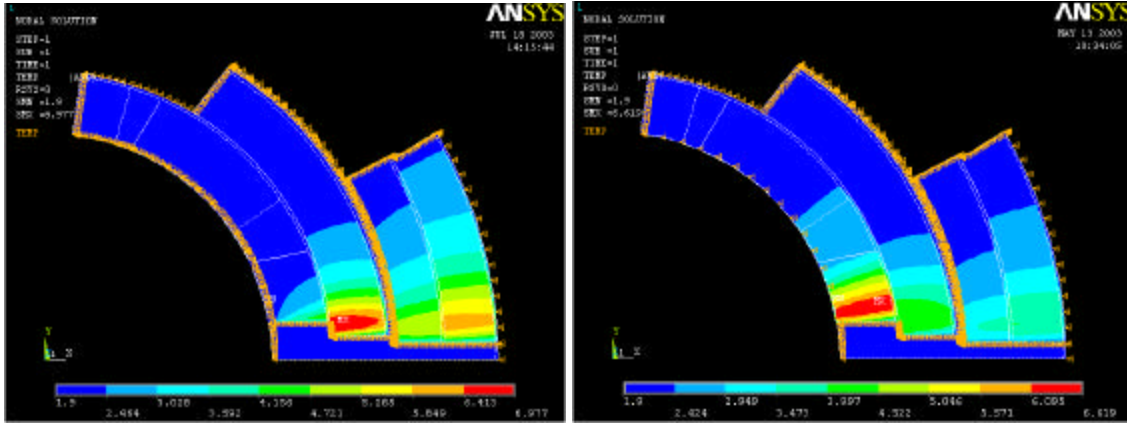


Figure 7: Temperature profile for the two cases: a) with interlayer cooling channels, He penetration in the coil mid-plane spacer and removed cable insulation on the inner surface of the mid-plane block in the innermost layer (left) and b) with standard cable insulation and reduced by a factor of two heat load (right).

6. Conclusions

A 2D finite element thermal analysis of the 4-layer Nb₃Sn separation dipole based on a cos-theta coil with thick midplane spacers, cooled by superfluid HeII at 1.9 K has been performed. The results show that a 4-layer magnet design without additional interlayer cooling does not provide adequate coil cooling with expected heat depositions. The point with maximum temperature of 22-28 K is located in the coil 2nd layer near the midplane spacer. With the interlayer cooling the point of maximum temperature is located in the innermost layer and coil maximum temperature could be kept below 12 K. The coil maximum temperature could be further reduced to a level of 6-7 K which is acceptable for Nb₃Sn coils by removing the insulation from the mid-plane block of the 1st (innermost) layer in order to provide direct contact with liquid HeII.

The results presented in this note were obtained with the assumption that the boundary conditions on the coil surface (HeII temperature) remain constant and

independent on the level of heat load. Providing of this condition in a practical design at the expected level of heat deposition in the coil certainly will challenge the design of D1 cold mass and cryogenics system for this IR configuration.

References

1. J.B. Strait et al., “Towards an new LHC interaction region design for a luminosity upgrade”, paper MOPA006, PAC2003, Portland (OR), 2003.
2. N. Mokhov et al., “Energy Deposition Limits in a Nb₃Sn Separation Dipole Placed in Front of the LHC High-Luminosity Inner Triplet”, paper TPPB065, PAC2003, Portland (OR), 2003.
3. N.V. Mokhov et al., “Protecting LHC IP1/IP5 Components Against Radiation Resulting from Colliding Beam Interactions”, Fermilab-FN-732 (2003), LHC Project Report 633 (2003).

Appendix

Table A1: Embedded Excel data for the applied heat loads.

Y/X (mm)	2	6	10	14	18	22	26	30	34	38	42	46	50	54	58	62
2	0.000000	0.000000	0.000000	0.000000	0.000000	0.000000	0.000000	0.000000	0.000000	0.000000	0.000000	0.000000	0.000000	0.000000	0.001854	0.645540
6	0.000000	0.000000	0.000000	0.000000	0.000000	0.000000	0.000000	0.000000	0.000000	0.000000	0.000000	0.000000	0.000000	0.000000	0.012089	0.430780
10	0.000000	0.000000	0.000000	0.000000	0.000000	0.000000	0.000000	0.000000	0.000000	0.000000	0.000000	0.000000	0.000000	0.000000	0.023359	0.286160
14	0.000000	0.000000	0.000000	0.000000	0.000000	0.000000	0.000000	0.000000	0.000000	0.000000	0.000000	0.000000	0.000000	0.000000	0.029764	0.208670
18	0.000000	0.000000	0.000000	0.000000	0.000000	0.000000	0.000000	0.000000	0.000000	0.000000	0.000000	0.000000	0.000000	0.000000	0.047747	0.116690
22	0.000000	0.000000	0.000000	0.000000	0.000000	0.000000	0.000000	0.000000	0.000000	0.000000	0.000000	0.000000	0.000000	0.001797	0.061264	0.038423
26	0.000000	0.000000	0.000000	0.000000	0.000000	0.000000	0.000000	0.000000	0.000000	0.000000	0.000000	0.000000	0.000000	0.009037	0.084210	0.018368
30	0.000000	0.000000	0.000000	0.000000	0.000000	0.000000	0.000000	0.000000	0.000000	0.000000	0.000000	0.000000	0.000785	0.026012	0.023212	0.014105
34	0.000000	0.000000	0.000000	0.000000	0.000000	0.000000	0.000000	0.000000	0.000000	0.000000	0.000000	0.000000	0.007490	0.034545	0.012810	0.008057
38	0.000000	0.000000	0.000000	0.000000	0.000000	0.000000	0.000000	0.000000	0.000000	0.000000	0.002695	0.019061	0.009450	0.005683	0.004776	
42	0.000000	0.000000	0.000000	0.000000	0.000000	0.000000	0.000000	0.000000	0.000000	0.000940	0.009751	0.010675	0.003711	0.004478	0.003079	
46	0.000000	0.000000	0.000000	0.000000	0.000000	0.000000	0.000000	0.000000	0.001099	0.014259	0.011319	0.005606	0.003297	0.003855	0.002528	
50	0.000000	0.000000	0.000000	0.000000	0.000000	0.000000	0.000000	0.000169	0.002334	0.008750	0.008890	0.004642	0.003385	0.002160	0.002407	0.002325
54	0.000000	0.000000	0.000000	0.000000	0.000000	0.000520	0.000810	0.011389	0.015638	0.003847	0.001579	0.002008	0.002531	0.001311	0.001950	0.002324
58	0.000006	0.000522	0.000481	0.000592	0.002127	0.004285	0.006358	0.003388	0.001226	0.001451	0.001670	0.002051	0.002499	0.002422	0.001497	0.001162
62	0.006796	0.014392	0.006822	0.008190	0.005558	0.002532	0.002332	0.002178	0.000949	0.001529	0.001313	0.001119	0.001209	0.002124	0.000809	0.001127
66	0.002150	0.003564	0.001924	0.002036	0.002815	0.002333	0.002428	0.001317	0.000790	0.000995	0.001124	0.000935	0.001539	0.000693	0.001579	0.002563
70	0.001824	0.000953	0.002318	0.001267	0.001464	0.001316	0.001948	0.000671	0.001042	0.000795	0.000689	0.000848	0.000766	0.000723	0.000665	0.002078
74	0.002068	0.001038	0.001407	0.000899	0.000728	0.001842	0.000862	0.000510	0.000538	0.001663	0.000473	0.000525	0.000644	0.000796	0.000458	0.000660
78	0.000496	0.001187	0.000580	0.000545	0.000541	0.001056	0.001769	0.000480	0.000553	0.002241	0.000437	0.000599	0.000759	0.000494	0.000555	0.001665
82	0.000427	0.000412	0.000599	0.000811	0.000561	0.000817	0.000568	0.000391	0.000623	0.000450	0.000512	0.000436	0.000387	0.000343	0.000569	0.000571
86	0.000504	0.000584	0.000520	0.000308	0.000338	0.000369	0.000373	0.000286	0.000517	0.000308	0.000277	0.000525	0.000711	0.000363	0.000501	0.000438
90	0.000406	0.000393	0.000422	0.000443	0.000356	0.000361	0.000311	0.000464	0.000264	0.000378	0.000359	0.000281	0.000386	0.000395	0.000388	0.000422
94	0.000315	0.000309	0.000357	0.000360	0.000353	0.000342	0.000475	0.000813	0.000289	0.000381	0.000325	0.000323	0.000299	0.000249	0.000336	0.000294
98	0.000185	0.000210	0.000217	0.000340	0.000452	0.000280	0.000233	0.000523	0.000259	0.000358	0.000298	0.000257	0.000562	0.000291	0.000252	0.000253